applied sciences

MDPI

Article

Retreat of an Ice Wall in Dobšiná Ice Cave (2018–2025): A Comparison of Three Change-Detection Methods Based on SfM Photogrammetry

Jakub Šveda, Katarína Pukanská, Karol Bartoš * and Ľubomír Kseňak

Institute of Geodesy, Cartography and GIS, Technical University of Košice, 04200 Košice, Slovakia; jakub.sveda@student.tuke.sk (J.Š.); katarina.pukanska@tuke.sk (K.P.); lubomir.ksenak@tuke.sk (Ľ.K.)
* Correspondence: karol.bartos@tuke.sk; Tel.: +421-55-602-2978

Featured Application

The presented workflow provides cave administrations with a low-cost, non-contact tool for long-term monitoring of vertical ice walls in show caves, where laser-based surveying is unreliable, and supports decisions on the protection of the ice fill.

Abstract

Perennial cave ice in the temperate zone is declining, and its monitoring requires suitable change-evaluation methods. This study compares three approaches to assessing the changes of a vertical ice wall in the Ruffínyi Corridor of Dobšiná Ice Cave (Slovakia), a UNESCO World Heritage Site, using a single multi-temporal dataset. Because the wall was inaccessible to tacheometry and laser scanning, we surveyed it using close-range Structure-from-Motion photogrammetry across seven annual epochs (2018–2023 and 2025). We evaluated changes relative to 2018 using cross-sections, M3C2 point cloud comparison, and vectorisation of five visible glacial layers. All three methods confirmed a predominant retreat of the wall. Cross-sections showed retreat of 40–176 mm (mean 113 mm) by 2025, the mean M3C2 distance reached −77.7 mm (≈12.9 mm/year), and the vectorised layers shifted by 72–214 mm (10–31 mm/year). Cross-sections and M3C2 independently identified a zone of local ice accumulation caused by water dripping from the ceiling (184 mm at one cross-section). The methods agree in the order of magnitude; differences reflect their spatial sampling. M3C2 provides the most complete area-wide assessment, cross-sections offer the simplest inspection and vectorisation, and a stratigraphically interpretable record; combined, they offer a more reliable basis for long-term monitoring of cave ice than any single method.

Keywords: cave ice; Dobšiná Ice Cave; Structure-from-Motion; photogrammetry; M3C2; vectorization; change monitoring

Check for updates

Academic Editor: Nathan J. Moore

Received: 1 October 2026
Revised: 20 October 2026
Accepted: 24 October 2026
Published: 28 October 2026

Copyright: © 2026 by the authors. Licensee MDPI, Basel, Switzerland. This article is an open access article distributed under the terms and conditions of the Creative Commons Attribution (CC BY) license.

1. Introduction

Cave ice constitutes a distinct category of underground ice formation. It forms where cave shape, microclimate, and airflow combine in the right way [1]. Because underground temperatures remain much more stable than on the surface, and because there is no direct sunlight, rain, or wind, cave ice preserves a valuable and exceptionally detailed record of the ancient climate. From the individual ice layers, it is possible to determine how summer temperatures and precipitation levels have changed over the last few centuries to millennia [2,3]. In recent decades, an increasing number of caves in temperate climate

zones have shown a gradual decline in their ice fill. This is also confirmed by systematic temperature measurements in four Alpine caves—Spannagelhöhle, Hundsalm, Rasslsystem and Schrattenhöhle—which have shown that global warming is not confined to the surface but is gradually penetrating underground as well. The air inside the caves is warming at approximately half the rate observed on the surface. The Hundsalm Cave is expected to lose its permanent ice fill entirely within ten years, whilst the nearby Spannagelhöhle lost its permanent ice as early as around 2002 [4]. A similar trend has also been documented in recent years in other European caves in temperate climate zones—for example, in the Vasto Cave in the Kanin massif in the Julian Alps on the Italian–Slovenian border [5], in the Peña Castil Cave in the Picos de Europa mountain range in Spain [6] or in the Scărișoara Cave in the Bihor Mountains in Romania [7].

Slovakia also has caves with significant ice loss: Silická Ice Cave [8] and Dobšiná Ice Cave. Dobšiná Ice Cave has been the subject of scientific research for more than 150 years. The first descent into the cave was made by the mining engineer Eugen Ruffíny in 1870 [9]. With a volume exceeding 110,000 m^3 of ice covering an area of over 9770 m^2, it is the world's second-largest ice-filled cave and one of the few large ice caves outside the Alpine region [9]. Radiocarbon analysis of bones from bats that perished in ice shows that this ice-filled cave responded differently to past climatic fluctuations than Alpine ice caves. Whilst the latter lost ice during the Medieval Climate Optimum, the ice in Dobšiná Ice Cave continued to accumulate during the same period [10,11]. Despite this historical stability, repeated geodetic surveys document a recent decline in the ice fill: between 2018 and 2023, floor-ice volume decreased by up to 667 m^3 in parts of the cave, and the ice surface lowered by 0.3–0.9 m in the Small Hall and Collapsed Dome [12]. Systematic speleoclimatic and glaciological monitoring of the cave has been carried out since 1990 [13].

Quantifying these changes requires repeated measurements that are comparable in terms of both space and time, which in practice also involves selecting a suitable method for data collection and processing. Digital photogrammetry is increasingly used to document such surfaces, particularly the Structure from Motion (SfM) method, which reconstructs a detailed 3D model from a series of overlapping photographs [14]. Similarly, point cloud comparison is also employed, as it enables repeatable, non-contact, and relatively straightforward measurements even in complex underground conditions [5]. Photogrammetry has already been validated in Dobšiná Ice Cave as a suitable method for spatially reconstructing challenging, highly reflective ice surfaces [15]. To assess changes between repeated measurements, the M3C2 method is also commonly used in the geosciences; it enables accurate comparison of two point clouds along the surface normal [16].

Research into and monitoring of ice caves today utilises a wide range of methods, from dating the ice and its organic inclusions (for example, radiocarbon dating of bat bones or plant remains) [17] to repeated geodetic and remote-sensing measurements of changes in surface and volume. Within Dobšiná Ice Cave itself, several measurement methods have already been compared simultaneously, including digital tacheometry, terrestrial laser scanning, digital photogrammetry using the Structure-from-Motion method, ground-penetrating radar, and microgravimetry. Photogrammetry is particularly suitable for locations that are difficult to access using conventional geodetic methods, and the M3C2 method is suitable for comparing point clouds between individual measurement stages [18]. A similar principle of comparing point clouds over time was also successfully applied in another Slovak ice cave, Silická ľadnica, in the Slovak Karst [8]. A similar approach, based on repeated ground-based laser scanning, was also used to monitor ice thickness in ice caves in Slovenia [19].

The aim of this study is to compare three different approaches to assessing changes in the surface of the ice wall in Dobšiná Ice Cave—the cross-section method, comparison

of point clouds using the M3C2 method, and the vectorisation of characteristic glacial layers—based on the same series of repeated measurements from 2018 to 2023 and 2025. The study focuses both on quantifying the changes themselves (retreat or, where applicable, local accumulation of ice) and on evaluating the advantages, limitations and mutual consistency of the results obtained using the individual methods, which may serve as a basis for selecting an appropriate approach for the future monitoring of similar cave ice formations.

The novelty of this study is threefold. First, point-cloud-based geomorphology shows that the choice of change-detection approach (DoD, C2C, C2M, M3C2, or object tracking) determines the direction of change measurement and, therefore, its magnitude and interpretation [16,20]. Studies of cave ice, however, have typically relied on one or two evaluation approaches without systematically assessing them against each other. Examples include cross-sections combined with 3D distances for floor ice in Silická ľadnica [8], repeated SfM-MVS surveys combined with GPR for ice deposits in the Julian Alps [5], and M3C2 in Dobšiná Ice Cave [12]. Previous comparative work in Dobšiná Ice Cave focused on data acquisition technologies [12,18]. To the best of our knowledge, this is the first study to systematically compare evaluation methods applied to the same multi-temporal SfM dataset of cave ice. Because the profile-based (cross-sections), surface-based (M3C2), and feature-based (layer vectorisation) approaches share identical input models and georeferencing, differences in their results can be attributed to the evaluation strategy rather than data acquisition. Second, researchers have so far used layering visible on exposed cave ice walls mainly as a stratigraphic and palaeoclimatic archive for layer identification, sampling, and dating [7,21]. Here, the boundaries of visible glacial layers serve as physically identifiable geometric markers, consistent with object-based change detection [20], so change is tracked on specific stratigraphic horizons rather than an undifferentiated surface. Third, the study addresses a vertical ice wall. Cave ice monitoring has so far concentrated on floor ice, ice extent and total ice volume [5,8,22], and TLS and photogrammetric studies of ice caves remain scarce overall [18]. On surface glaciers, steep ice faces have been shown to require dedicated change-detection approaches [23]. Comparable cave surfaces, however, remain largely unaddressed, partly because laser-based methods are compromised by beam penetration into the ice [12]. With seven annual epochs spanning 2018–2025, the dataset extends the previously published 2018–2023 record from this site [12] and provides a basis for selecting an appropriate evaluation method for the long-term monitoring of similar cave ice formations.

2. Locality of the Case Study

The Dobšiná Ice Cave is located in the Slovak Paradise National Park (Slovak Republic) (Figure 1) and is one of the world's most significant ice-filled caves. It is one of the few examples of extensive underground ice formation originating in a mid-mountain location within a temperate climate zone, outside the typical Alpine environment where cave ice is commonly found [24].

The cave is situated within the cadastral area of the town of Dobšiná, in the Slovak Paradise National Park. It was discovered in 1870 by the mining engineer Eugen Ruffinyi and, in 1882, became the first electrically lit cave in Hungary. In 2000, it became part of a UNESCO World Natural Heritage Site [25]. With its length (1232 m) and depth (112 m), it ranks among the largest ice caves in Europe. The cave is unique because its underground glacier is at a lower altitude (920 to 950 m) and it lies outside the Alpine region, whereas ice caves in the Alps are situated at 1420 m above sea level [26].

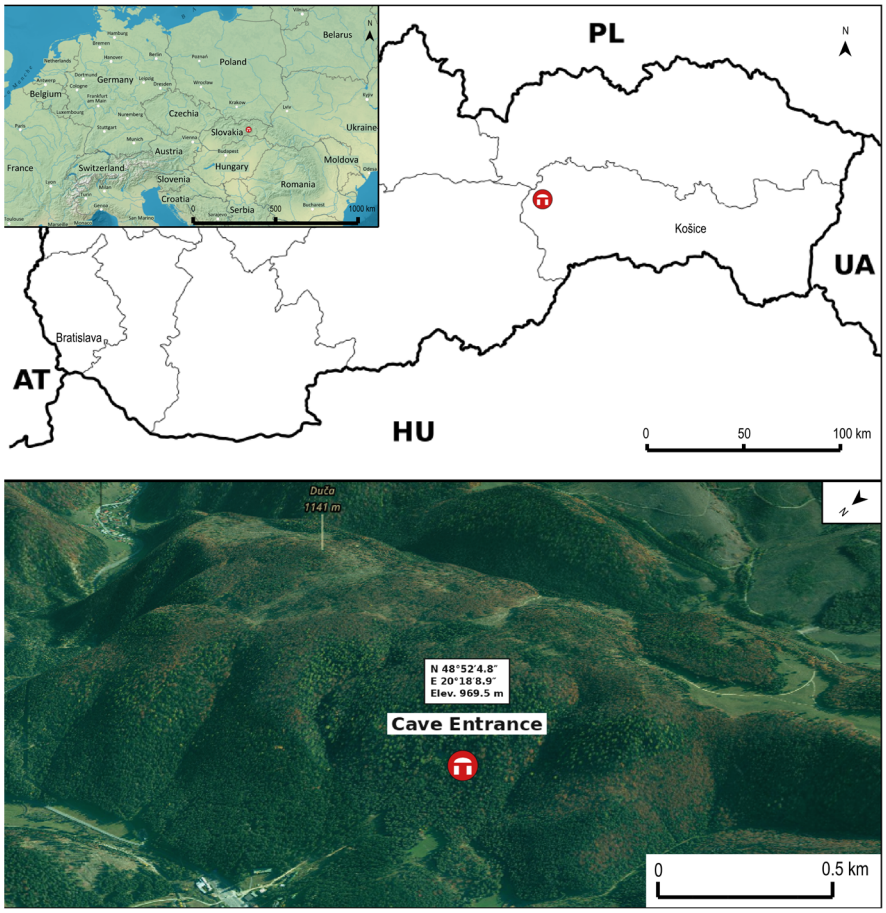

Figure 1. Location of Dobšiná Ice Cave in Slovakia [27,28].

The entrance to the cave, known as the 'Ice Hole', is located 969.5 m below the summit of Duča. In the cave's lower chambers, 70 m below the entrance, the temperature remains below freezing year-round. In some places (the Great Hall), the ice reaches 26.5 m thick, with an estimated volume of 110,000 m^3. The underground glacier in the cave forms by natural cooling, with ice deposits taking the form of ice columns and stalagmites, floor ice, and icefalls. The main sections of the cave include the Great Hall and the Small Hall, Ruffinyi's Corridor and the Collapsed Dome (Figure 2a,b). The cave is open to the public via a 515 m route with a 43 m vertical rise [25,26].

Scientific research into the cave's ice fill dates to the 1870s. Shortly after the cave's discovery, J. Fehér (1870–1871) made the first observations; J. E. Pelech subsequently estimated, in 1878–1879, the ice fill area at approximately 7171 m^2 and its volume at 125,000 m^3 [29]. In the mid-20th century, A. Droppa (1950–1955), based on detailed geodetic surveys and the calculation of annual ice layers (3–5 mm thick), estimated a new area of approximately 11,200 m^2 and a volume of about 145,000 m^3, with the ice thickness ranging from 0.5 m at the entrance to 25 m in the Great Hall [29]. More precise geophysical and geodetic measurements carried out by J. Géczy and L. Kucharič in 1995 subsequently established the reference values still in use today—an ice volume of 110,132 m^3, an ice-filled area of 9772 m^2 and a maximum ice thickness of 26.5 m [24], which are also supported by systematic monitoring carried out since 1990 [13].

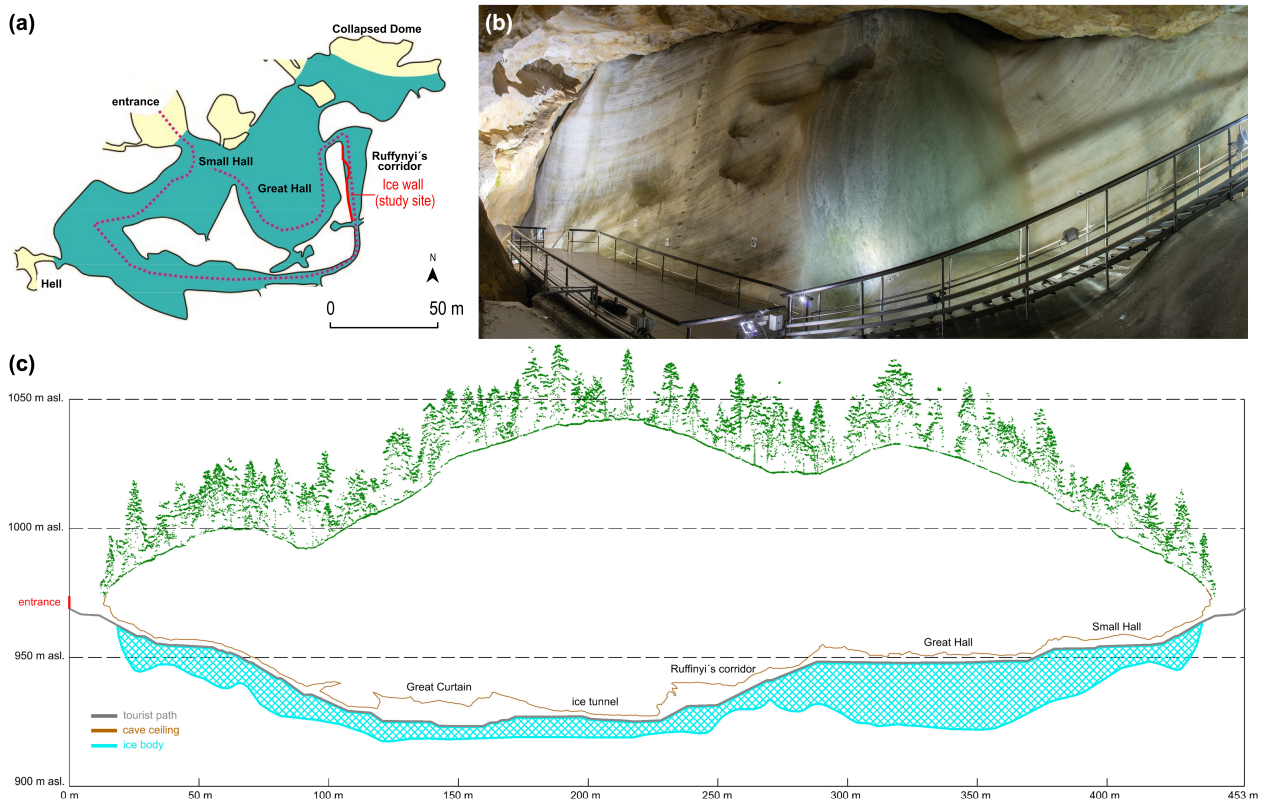

Figure 2. (**a**) Plan view of Dobšiná Ice Cave showing the location of the studied ice wall in Ruffinyi's Corridor [30]; (**b**) view of the ice wall in Dobšiná Ice Cave; (**c**) a longitudinal cross-section through the cave (source of the terrain—LiDAR data: ÚGKK SR) (after [12]).

This research focuses on the vertical ice wall in the Ruffinyi Corridor (Figure 2c), which reaches approximately 10 m in height and consists of layered ice [18]. Given the extent of this vertical surface, the significant elevation differences, and the limited space for movement, conventional tacheometry or terrestrial laser scanning cannot be used at this site; therefore, digital photogrammetry using the Structure from Motion method is employed to document and monitor changes [12]. Repeated measurements between 2018 and 2023 recorded localised ice-volume losses of up to 9 m^3 on this wall [12], confirming the need for a more precise, systematic assessment of its changes, which this study focuses on.

Climate Conditions in the Ruffinyi Corridor

Temperature conditions are currently documented by continuous measurements taken by climatologists from the Slovak Caves Administration in the Ruffinyi Corridor between January 2018 and July 2026 (Figure 3). This includes 2108 daily averages, representing about two-thirds of the period. The average monthly temperature for the entire period is −0.34 °C. In years with almost complete coverage, the average annual temperature was −0.48 °C (2018), −0.15 °C (2020) and −0.30 °C (2025). The annual cycle is markedly asymmetrical:

Winter: the coldest months are January to March, with monthly averages ranging from −1.04 °C to −1.29 °C (February). During cold snaps, daily averages have fallen as low as −4.43 °C (1 March 2018).

Summer and autumn: from June to October, temperatures remain just above freezing, with monthly averages ranging from +0.01 °C to +0.14 °C (August). The highest daily average for the entire period was just +0.47 °C (20 July 2022).

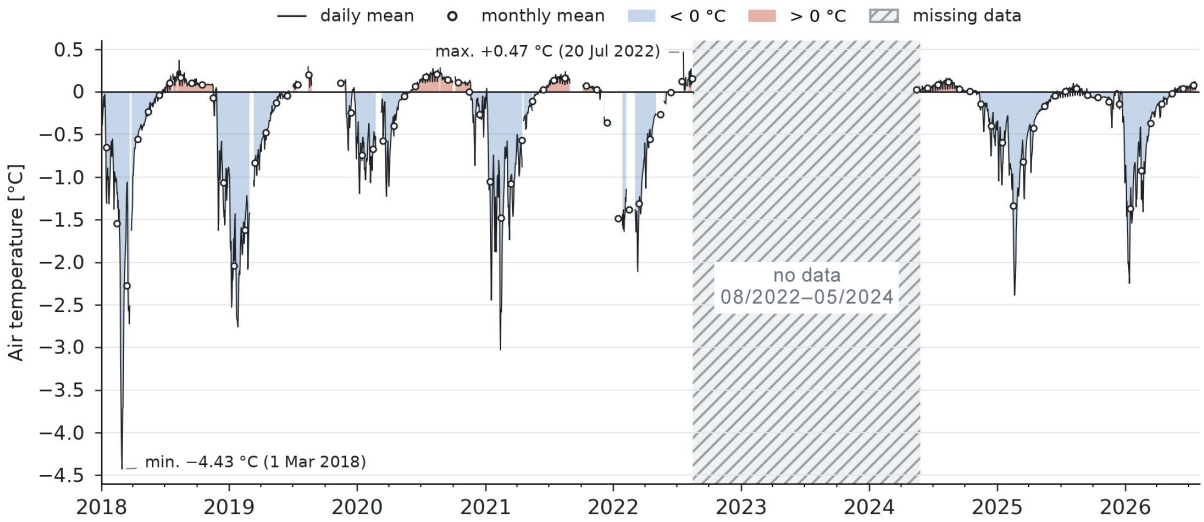

Figure 3. Overview of daily mean temperatures in the Ruffinyi Corridor between 1 January 2018 and 23 July 2026.

The air temperature was below 0 °C on 62.5 percent of days. Winter temperatures varied significantly from year to year. The average for December to March was −1.45 °C in winter 2017/18 and only −0.54 °C in winter 2019/20, when the temperature fell below −1 °C on only 9 days (compared with 75 days in 2018). Relative humidity (monthly data for 2018–2022) averaged 97.6 percent. From May to November, the air was practically saturated (99–100 percent); from January to March, humidity fell to 93–94 percent as drier, colder air flowed into the cave. Temperature and humidity are closely correlated (r = 0.87). This pattern is consistent with a model of winter cooling and summer air stagnation in the cave. The same mechanism has also been described in other ice caves, e.g., the Eisriesenwelt [31] and Scărișoara, where the temperature in the Great Hall ranges from +0.1 °C in summer to −14.7 °C in winter [32]. In summer, temperatures slightly above freezing and moisture-saturated air create conditions for surface melting of the ice.

3. Materials and Methods

Three independent methods were used to assess changes in the surface of the ice wall, applied to the same series of repeated measurements (2018–2023 and 2025; no measurements were taken in 2024): the cross-section method, comparison of point clouds using the M3C2 method, and vectorisation of characteristic glacial layers.

3.1. Geodetic Survey

The geodetic survey of the Dobšiná Ice Cave began in 2011, initiated by the Slovak Caves Administration. The first step was to monument the underground geodetic point field, survey it using a closed traverse, and then perform an adjustment. The network is referenced to the Slovak national coordinate system S-JTSK and the national vertical reference Bpv via surface control points forming a baseline approximately 1047 m apart. These points were determined using the static GNSS method, utilising the SKPOS service during three-hour observations. From these, we subsequently determined the underground points 5004–5012; these were monumented with survey pegs in solid, unweathered sections of the rock ceiling, and some were marked with retroreflective targets. The adjusted network achieved a mean positional error of 4.9 mm, a mean coordinate error of 3.5 mm and a mean height error of 1.7 mm [12]. Since 2018, the geodetic point field has gradually expanded to include drilled mining survey marks with reflective targets and new points on the cave walls and ceiling. The ground control points and check points for photogrammetric surveying in

the Ruffínyi Corridor are also linked to this network via a total station. The a priori accuracy of the total station measurement of the photogrammetric points (Leica Viva TS15 total station (Leica Geosystems AG, Heerbrugg, Switzerland), reflectorless mode, two faces, free station with $\sigma_{X,Y,Z} = 1$ mm and $\sigma_{\omega} = 1$ mgon), relative to the underground geodetic point field, is defined by the mean positional error $m_p \leq 2.5$ mm and the mean error derived for trigonometrical measurement of heights $m_h \leq 1.5$ mm.

3.2. Digital Close-Range Photogrammetry

The vertical ice wall in the Ruffínyi Corridor was surveyed using digital close-range photogrammetry via the Structure-from-Motion (SfM) method. Neither total station surveying nor TLS is applicable here because of the extent of the vertical surface, large elevation differences, limited space for movement, and laser penetration into the ice. The SfM method derives an object's spatial geometry from a set of overlapping images taken from different viewpoints. It performs image pairing, bundle registration with camera self-calibration, and dense multi-image reconstruction in a single processing pipeline [33,34]. The analysis includes seven annual epochs (2018–2023 and 2025), with images always captured in autumn (October–November).

For the 2018–2023 epochs, we used a Pentax K-5 DSLR with an APS-C sensor and a Pentax SMC DA 15 mm f/4 ED AL Limited lens (both Ricoh Imaging Company, Ltd., Tokyo, Japan). In 2025, we used a full-frame Pentax K-1 Mark II DSLR camera with an HD Pentax-D FA 21 mm f/2.4 ED Limited DC WR lens (Ricoh Imaging Company, Ltd.). Both set-ups provide a comparable field of view (equivalent focal lengths of ≈23 mm and 21 mm, respectively). No simultaneous acquisition with both set-ups was carried out; the possible influence of the camera change on the results is discussed in Section 5. We captured the images from a tripod using a self-timer in RAW format and subsequently processed them in Agisoft MetaShape® Professional Edition, Version 1.6.0 software (Agisoft LLC, St. Petersburg, Russia, 2019) using a standard procedure [15]. We georeferenced the models to control points marked with coded targets and surveyed with a total station. Processing statistics for each epoch are given in Table 1. Each epoch produces a dense point cloud, a polygonal model, and an orthophotomosaic of the wall.

Table 1. Parameters of imaging and image processing for photogrammetric survey.

	1st Stage (11/2018) *	**2nd Stage (11/2019) ***	**3rd Stage (10/2020) ***	**4th Stage (10/2021) ***	**5th Stage (10/2022) ***	**6th Stage (11/2023) ***	**7th Stage (10/2025) ****
No. of images used	50	76	106	138	105	77	94
Average imaging distances	9.4 m	8.4 m	6.0 m	5.5 m	6.2 m	6.3 m	5.8 m
No. of tie points [1]	21,585	17,069	125,278	81,253	49,925	104,267	169,858
No. of reconstructed points	21 mils.	23 mils.	23 mils.	42 mils.	32 mils.	36 mils.	103 mils.
Ground Sample Distance [2]	2.4 mm	2.3 mm	1.9 mm	2.2 mm	2.2 mm	3.0 mm	2.0 mm
Maximal error [3]	2.95 pix	1.45 pix	1.44 pix	1.50 pix	1.06 pix	3.51 pix	2.10 pix
Reprojection error [4]	0.55 pix	0.35 pix	0.264 pix	0.34 pix	0.30 pix	0.51 pix	0.44 pix
No. of markers	10	7	9	10	10	10	9

Table 1. *Cont.*

	1st Stage (11/2018) *	2nd Stage (11/2019) *	3rd Stage (10/2020) *	4th Stage (10/2021) *	5th Stage (10/2022) *	6th Stage (11/2023) *	7th Stage (10/2025) **
No. of Ground Control Points	4	4	6	6	6	6	6
Accuracy in the reference s. [5] (Total error)	3.3 mm	5.0 mm	2.6 mm	3.5 mm	4.3 mm	4.9 mm	1.4 mm

[1] tie points represent matches between key points detected on two or more different images; [2] pixel size in object space units; [3] distance between the point on the image where a reconstructed 3D point can be projected, and the original projection of that 3D point detected on the photo and used as a basis for the 3D point reconstruction procedure; [4] root mean square reprojection error averaged over all tie points on all images; [5] root mean square error of all the GCPs; * imaged by DSLR Pentax K-5 with Pentax SMC DA 15 mm f/4 ED AL Limited; ** imaged by FullFrame DSLR Pentax K-1 Mark II with Pentax HD Pentax-D FA 21mm f/2.4ED Ltd. DC WR.

3.3. The Cross-Section Method

Changes to the surface of the ice wall were analysed using the cross-section method. Five cross-sections were defined on the ice wall: four vertical (A–A′ to D–D′) and one horizontal (E–E′), positioned to cover representative parts of the wall, including areas with visually distinct dynamics of change (Figure 4). For each measurement phase in the years 2018–2023 and 2025 (no measurements were taken in 2024), a wall profile was generated from the photogrammetric 3D model along the cross-section line (vertical for cross-sections A–A′ to D–D′, horizontal for cross-section E–E′). The profiles from all phases were then displayed together in a single graphical output for each section (colour-coded by measurement year; see Section 4.1). On each section, characteristic points (e.g., A1–A3, B1–B3, C1, D1–D2, E1–E4) were identified at locations where the gap between the line from the 2018 reference stage and the line from the 2025 stage was most clearly visible on the profile graph. Where the gaps were smaller, these locations were supplemented with an enlarged inset for better legibility. At these points, the perpendicular distance between the 2018 cross-section and the 2025 cross-section was measured directly in the CloudCompare software using the Point picking/Point list picking tool. The scale and orientation of the coordinate axes are specified in each graphical output.

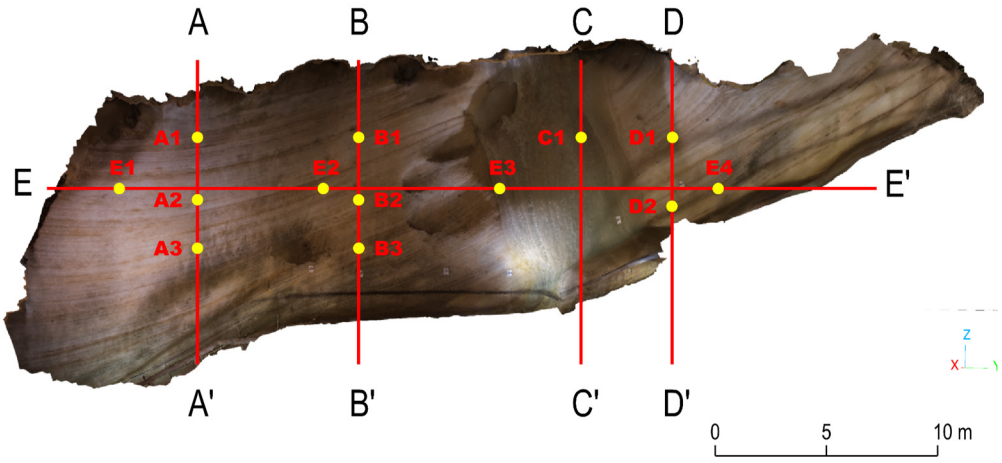

Figure 4. Location of the five cross-sections (A–A′ to E–E′) established across the ice wall, with the position of individual measurement points along each section (e.g., A1–A3, B1–B3, C1, D1–D2, E1–E4).

3.4. The M3C2 Method (Multiscale Model-to-Model Cloud Comparison)

The M3C2 method (Multiscale Model-to-Model Cloud Comparison [16]), implemented in the CloudCompare software v2.14beta [35], was used to compare the stages; this method directly determines the distance between two point clouds, without interpolating into a mesh or raster. The distance is measured along the local surface normal, allowing accurate evaluation even on steep and geometrically complex surfaces. The calculation takes place at the core points i. At each of these, the normal $\hat{n}_i$ is determined from the points of the reference point cloud within a radius of D using the principal components method. In the multiscale approach, D is selected from a set of candidate radii such that the surface is as flat as possible at the given scale. A projection cylinder with a radius of $D/2$ is created along the normal, and the points of both point clouds lying within the cylinder are projected onto its axis. The distance M3C2 is the difference between the average positions of the points of both point clouds on the axis:

$$L_{M3C2}(i) = (\overline{x}_2 - \overline{x}_1)\hat{n}_i, \tag{1}$$

For each distance, a detection threshold is determined at a 95 percent confidence level:

$$LoD_{95}(i) = \pm 1.96\left(\sqrt{\frac{\sigma_1^2(i)}{n_1(i)} + \frac{\sigma_2^2(i)}{n_2(i)}} + reg\right) \tag{2}$$

where σ_1 and σ_2 are the standard deviations of the points in both point clouds within the cylinder along the normal, n_1 and n_2 are their respective numbers, and reg is the systematic error in the mutual registration of the point clouds. A change is considered demonstrable if $|L_{M3C2}| > LoD_{95}$. For dense point clouds, the statistical term in Equation (2) is negligible and does not consider the spatial correlation of errors; therefore, the detection threshold is determined predominantly by the reg term.

Point clouds from photogrammetric processing with Agisoft Metashape® Professional Edition, Version 1.6.0 software (Agisoft LLC, St. Petersburg, Russia, 2019) were used as input data for the individual surveys carried out in 2018–2023 and 2025 (no survey was carried out in 2024). The point clouds were georeferenced to common control points, achieving spatial alignment between the point clouds from the individual stages without additional registration. The year 2018, i.e., the oldest available point cloud, was designated as the reference stage. The perpendicular distance relative to this reference was then determined for each subsequent stage using the M3C2 method. The calculation parameters (mean of the normal and mean of the projection) were determined automatically using the 'Guess parameters' function, based on the average point spacing.

For each point, the output included the M3C2 distance value, its uncertainty (distance uncertainty), and a Boolean flag indicating a significant change. A point was classified as having undergone a significant change if the absolute value of its M3C2 distance exceeded the combined uncertainty of both compared point clouds at a 95 percent confidence level. The proportion of such points in the individual stages ranged from 96.4 percent (2020) to 99.4 percent (2025), suggesting that the changes recorded on the wall's surface were not random noise, but a widespread and statistically verifiable phenomenon.

The resulting values were exported in ASCII format and processed in Python 3.14 (Python Software Foundation, Beaverton, OR, USA), where we calculated the mean, median, and standard deviation of the M3C2 distance; the average measurement uncertainty; and the proportion of points showing a statistically significant change for each year.

3.5. Vectorisation of Glacial Layers

The third method used to assess changes in the ice wall was vectorisation. For each measurement phase (2018–2023, 2025; no measurements were taken in 2024), the boundaries

of five characteristic glacial layers (Figure 5; A–E) were manually vectorised as polylines in 3D Survey software (3Dsurvey, version 4.1.1, 3Dsurvey d.o.o., Ljubljana, Slovenia), based on a photogrammetric 3D model of the wall. The vectorised lines were subsequently exported to MicroStation software (MicroStation V8i, version 08.11.09, Bentley Systems, Inc., Exton, PA, USA), from where the spatial coordinates (X, Y, Z) of the individual vertices were exported to a spreadsheet file (Excel), separately for each measurement phase and each layer.

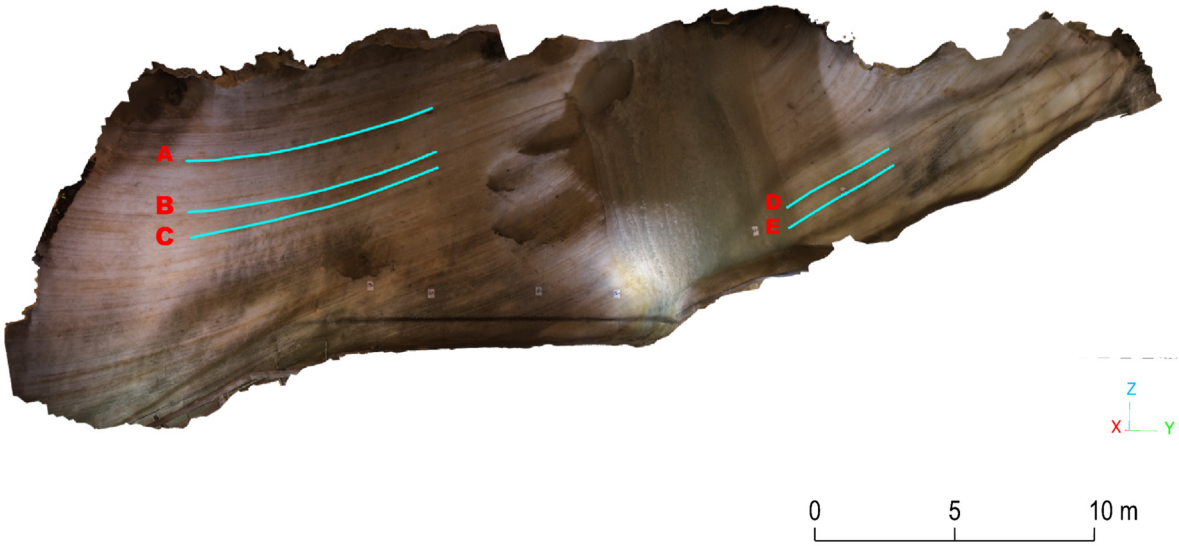

Figure 5. Overview of the vectorised layers A–E on the ice wall.

The accuracy of the coordinates prepared in this way was verified by cross-checking prior to further processing—the values in Excel were compared point by point with the original text exports from MicroStation.

Because the number and distribution of vectorised points differed slightly between stages, we could not directly compare points with the same serial number.

The difference between two stages of a given layer was therefore determined for each point as the shortest distance to the nearest point on the polyline of the compared stage (the so-called 'nearest neighbour' method), rather than simply to the nearest vertex. Because it was necessary to work with all three coordinates (X, Y, and Z) simultaneously, we calculated the shortest 3D distance between a point and a line using a custom Python script.

As with the cross-section method and M3C2, the year 2018 was set as the reference stage. In addition to the cumulative change relative to this reference, we also calculated the average annual rate of change (mm/year) to ensure comparable time intervals between stages (the 2023–2025 interval is a two-year period due to the absence of measurements in 2024).

4. Results

All three methods were applied to the same series of seven photogrammetric models (2018–2023 and 2025), whose processing parameters are summarised in Table 1. The models achieved a ground sample distance of 1.9–3.0 mm, a reprojection error of 0.26–0.55 pix, and a total GCP error of 1.4–5.0 mm, all considerably smaller than the cumulative changes evaluated below. In all methods, the 2018 epoch served as the reference, and changes are expressed relative to it; where rates are given, they are normalised by the number of years since the reference epoch. M3C2 distances are signed, with negative values indicating retreat of the ice surface (ice loss) and positive values indicating accumulation. The cross-

section and vectorisation methods yield unsigned distances; we therefore determined the direction of change from the profile graphs and the height component (ΔZ), respectively. We present the results separately for each method in Sections 4.1–4.3, and evaluate their mutual consistency in the Discussion.

4.1. The Cross-Section Method

Measurements taken at five transverse profiles (A–A′ to E–E′; Figures 4 and 6) between the 2018 reference stage and the 2025 stage revealed two distinct processes. On profiles A–A′, B–B′, D–D′ and E–E′, a clear retreat of the ice wall was recorded, with values ranging from 40 to 176 mm (average 113 mm, Table 2). The greatest retreat was measured at profile B–B′ (point B1, 176 mm), and the smallest at profile D–D′ (point D2, 40 mm). Profiles A and B on the left-hand side of the wall show similar, slightly higher average retreat values (123–131 mm) compared with profile D (63 mm); profile E–E′ (a horizontal section across the entire wall) averages 115 mm. A vertical gradient is also evident within profiles A, B and D—the highest point on each profile (e.g., A1, B1, D1) shows greater retraction than the lower points.

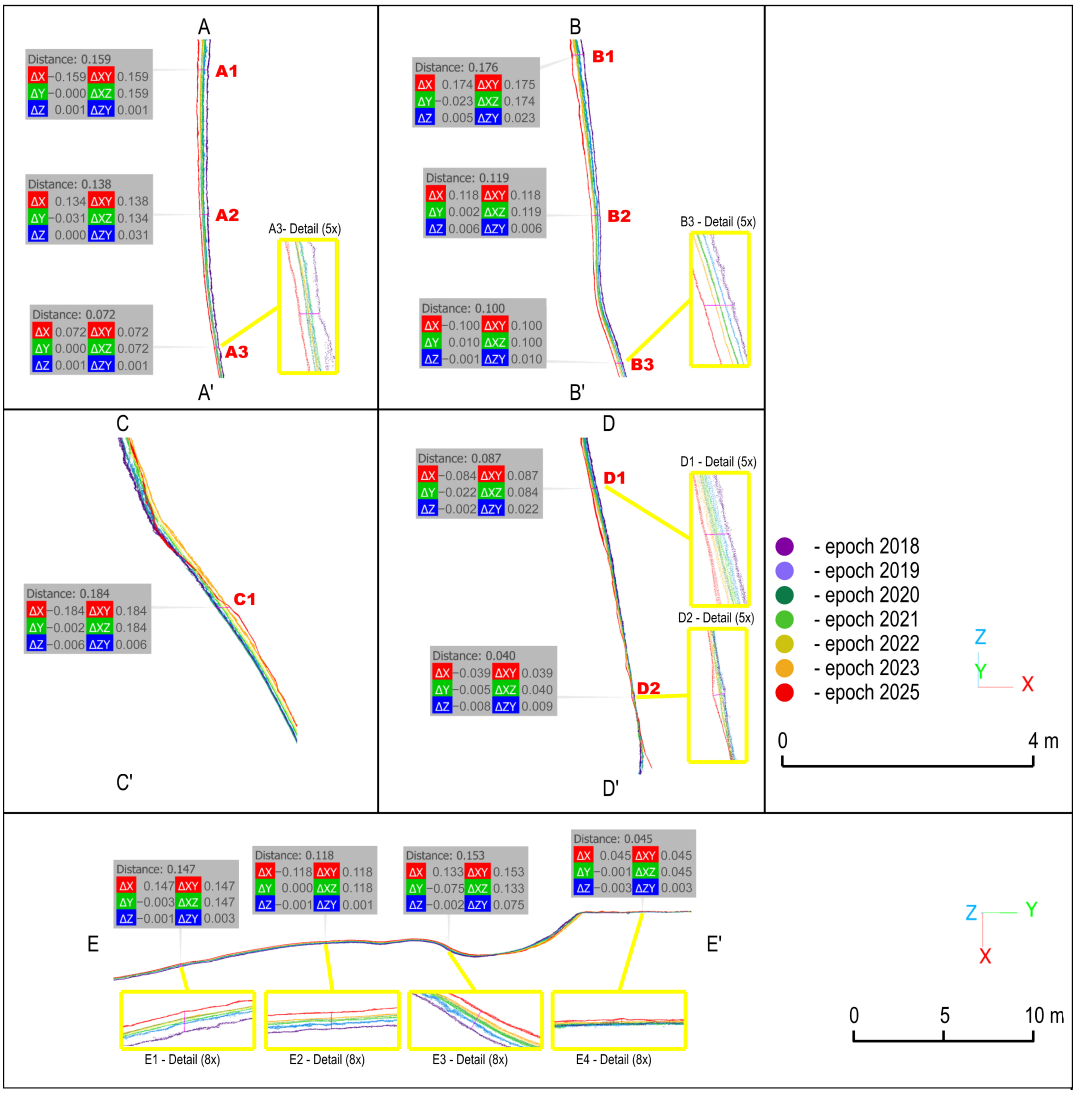

Figure 6. Cross-sections A–A′ to E–E′ across the ice wall, showing wall profiles for all surveyed epochs (2018–2023, 2025; colour-coded by year).

Table 2. Cross-section of the ice wall—measured displacement (2018 vs. 2025).

Cross-Section	Point	Distance [mm]	Average [mm]	Character
A–A′	A1	159	123	retreat
A–A′	A2	138		retreat
A–A′	A3	72		retreat
B–B′	B1	176	131	retreat
B–B′	B2	119		retreat
B–B′	B3	100		retreat
C–C′	C1	184	184	accumulation
D–D′	D1	87	63	retreat
D–D′	D2	40		retreat
E–E′	E1	147	115	retreat
E–E′	E2	118		retreat
E–E′	E3	153		retreat
E–E′	E4	45		retreat

Profile C–C′ (point C1, 184 mm; Table 2) differs in terms of interpretation. At this point, water drips through the cave ceiling, causing localised freezing and increasing the thickness of the ice layer, so this is not ice loss but accumulation. The value of 184 mm thus represents the greatest local change among all five profiles, albeit with the opposite sign compared to the other four profiles.

4.2. M3C2 Method

The M3C2 analysis confirmed a gradual retreat of the ice wall in all monitored stages compared with the reference year 2018 (Table 3). The cumulative average change in distance increased from −20.1 mm in 2019 to −69.9 mm in 2025, with the greatest increase recorded between 2023 and 2025 (from −38.3 mm to −69.9 mm). The annual rate of change was not constant—it was highest immediately after monitoring began (−21.4 mm/year in 2020), then slowed down (approximately −8 to −10 mm/year in 2021–2023) and accelerated slightly towards 2025 (−9.98 mm/year; average for the entire period −12.96 mm/year). The standard deviation increased with the length of the period under consideration (from 35 mm in 2019 to 103.3 mm in 2025), reflecting the increasing spatial heterogeneity of the retreat across the wall. The average measurement uncertainty remained low and stable throughout the entire period (1.3–1.9 mm), i.e., one to two orders of magnitude lower than the measured changes. A statistically significant change was recorded at 96.4–99.4 percent of the compared points in all stages, confirming that the recorded changes are genuine and not the result of measurement noise.

The spatial distribution of changes over the entire period 2018–2025 (Figure 7) shows that the retreat was not uniform across the face. Most of the area shows a slight to moderate decrease (green to yellow shades, approx. −0.05 to −0.15 m), while a marked anomaly (orange–red shades) occurs in the eastern part of the corridor. This anomaly corresponds to the point where water flows in from the cave ceiling—therefore, at this point, there is not a loss but, on the contrary, an accumulation of ice, which is consistent with the findings from cross-section C–C′ (Figure 6).

Table 3. Changes in the ice wall surface (2018–2025)—point cloud comparison using the M3C2 method.

Reference Epoch 2018								
Survey Year	**Years Since Reference**	**Mean M3C2 Distance [mm]**	**Median [mm]**	**Standard Deviation [mm]**	**Rate of Change [mm/yr]**	**Mean Uncertainty [mm]**	**Number of Points (Core Points)**	**Points with Significant Change [%]**
2019	1	−20.10	−25.00	35.00	−20.10	1.91	165,347	96.6
2020	2	−42.80	−46.4	46.90	−21.40	1.34	162,253	96.4
2021	3	−29.10	−37.00	49.70	−9.70	1.62	163,424	97.5
2022	4	−35.60	−43.20	59.50	−8.90	1.65	164,041	97.9
2023	5	−38.30	−54.60	77.90	−7.66	1.55	158,693	97.9
2025	7	−69.90	−87.40	103.3	−9.98	1.43	165,912	99.4
Avg.					−12.96			

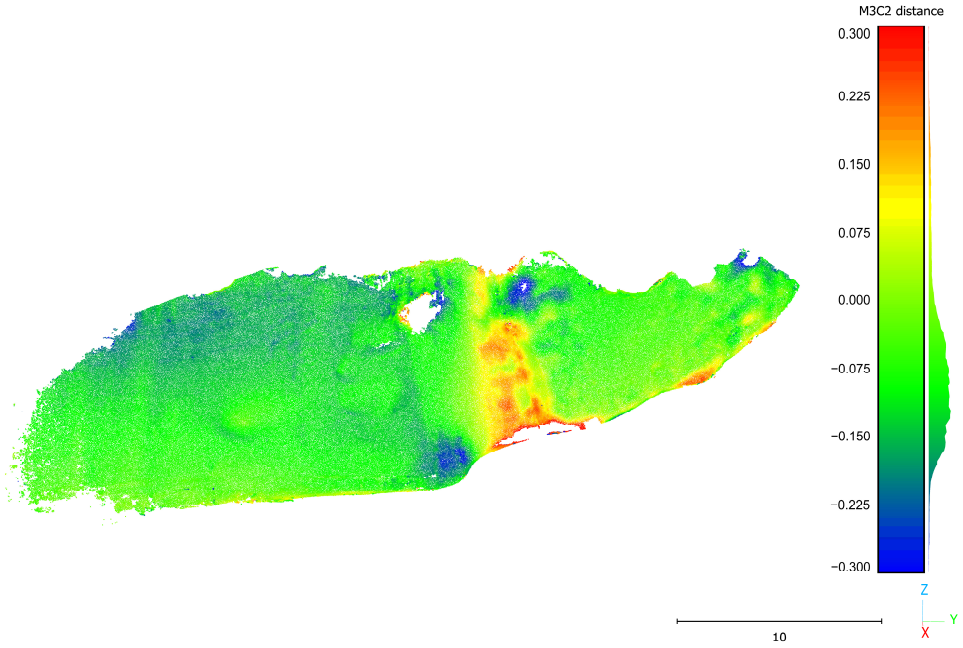

Figure 7. The spatial distribution of change over the full 2018–2025 period.

4.3. Vectorisation Method

Vectorisation of the five glacial layers (A–E; Figure 5) confirmed the retreat of the ice wall between the 2018 reference stage and the 2025 stage across all five monitored layers (Table 4). The average 3D distance (horizontal and vertical displacement combined) ranged from 72.0 to 214.2 mm across the layers, corresponding to a rate of 10.3–30.6 mm/year. The values decrease progressively from layer A (214.2 mm; 30.6 mm/year) towards layer E (72.0 mm; 10.3 mm/year), with layers A, B and C showing a more pronounced relative retreat than layers D and E.

A supplementary analysis of the vertical component of the change (ΔZ, Table 4) essentially confirms the same trend—layers A and C recorded the greatest decrease in height (−107.4 to −154.2 mm), layers B and D showed a moderate decrease (−100.2 and −102.3 mm, respectively), and layer E showed a significantly smaller decrease (−33.7 mm). Because the 3D distance is unsigned and cannot, on its own, distinguish between retreat and potential accumulation, we used the height component (ΔZ) to confirm the direction of change, confirming a decrease in height (i.e., retreat) for all five layers, albeit to varying degrees.

Table 4. Results of the vectorisation method.

Reference Epoch 2018							
Layer	**Years Since Reference**	**Mean Distance [mm]**	**Median [mm]**	**Standard Deviation [mm]**	**Rate of Change [mm/yr]**	**Number of Points**	**ΔZ Height Change [mm]**
A	7	214.2	217.9	23.6	30.6	9	−154.2
B	7	168.7	157.9	18.4	24.1	9	−100.2
C	7	147.2	141.6	11.3	21.0	9	−107.4
D	7	106.4	120.2	25.0	15.2	5	−102.3
E	7	72.0	86.1	26.0	10.3	5	−33.7

5. Discussion

The three methods used differ both in the way the data being compared is collected and in the spatial coverage of the wall. Both the cross-section method and vectorisation use a limited, manually defined set of points or lines (cross-section method: 13 points on five profiles; vectorisation: five lines with 5–9 points each). In contrast, the M3C2 method compares the entire point cloud, thereby providing a comprehensive, statistically grounded assessment of changes, including an estimate of measurement uncertainty and the proportion of statistically significant points. Cross-sections and vectorisation, by contrast, allow simpler, faster manual inspection at predefined locations on the wall.

In addition to the direction of change, its rate must also be compared. The average retreat measured using the cross-section method (113 mm over the period 2018–2025, i.e., approximately 16 mm/year) is higher than the average cumulative value from the M3C2 method (−69.9 mm; an average of 12.96 mm/year), whilst vectorisation yielded values for individual glacial layers ranging from 10.3 to 30.6 mm/year, thus encompassing the results of both other methods. Despite their different data collection methods, all three methods agree on the order of magnitude of the change (units to low tens of mm/year), which can be regarded as mutual confirmation. The higher cross-section value is expected; characteristic points on the profiles were deliberately selected where the difference between the 2018 and 2025 stages was most clearly visible, whereas M3C2 averages across the entire wall surface, including less dynamic areas. The cross-sections and vectorisation therefore tend to capture local maxima of change at selected points, whilst M3C2 provides an area-wide average; the difference in the measured values thus reflects different spatial data selection strategies, not a discrepancy between the methods themselves.

At the same time, vectorisation required a specific methodological approach. As the number and position of the vectorised points varied between stages, it was necessary to use a custom calculation of the shortest 3D distance between a point and a neighbouring line (the nearest neighbour method, taking into account X, Y and Z), since standard GIS tools for finding the nearest neighbour generally operate only in the X-Y plane.

Both the cross-section method and the M3C2 method independently identified the same location of local ice accumulation caused by refreezing water running down the cave ceiling (profile C–C′; Figures 4 and 6), providing mutual confirmation of this finding. The vectorised layers do not cover this specific location; therefore, this phenomenon was not recorded separately in their results. A similar phenomenon of local ice accumulation caused by the refreezing of water within the cave has also been documented through repeated measurements in another Slovak ice cave—Silická ľadnica [36,37], which suggests that this is not merely a local peculiarity of the Dobšiná Ice Cave, but a more widespread process in cave ice systems within the temperate climate zone.

Also noteworthy is the unevenness of the annual retreat rate determined using the M3C2 method (Chapter 4.2)—the highest value was recorded in the very first year of observation (−21.4 mm/year in 2020), followed by a slowdown to approximately −8 to −10 mm/year in the years 2021–2023. Because average measurement uncertainty remained low and stable throughout the period (1.3–1.9 mm), this is unlikely to be an artefact of measurement inaccuracy; rather, it reflects interannual climatic variability, which is also reflected, with a certain delay, in the cave's underground microclimate. Because no measurements were taken in 2024, it is not possible to conclusively verify whether this represents a short-term fluctuation or the start of a longer-term trend reversal, highlighting the importance of continuous, uninterrupted monitoring to distinguish interannual fluctuations from an actual retreat trend reliably.

The change in camera system in 2025 (Section 3.2) is a potential source of systematic differences between the 2025 epoch and the previous ones, which could not be verified directly, as no simultaneous acquisition with both set-ups was carried out. The processing statistics, however, do not indicate any deterioration:

1. Both set-ups were processed using the same SfM workflow and georeferenced to the same network of control points surveyed by a total station;
2. The 2025 model achieved a ground sample distance of 2.0 mm, a reprojection error of 0.44 pix and a total GCP error of 1.4 mm, i.e., values within or better than the range of the 2018–2023 epochs (1.9–3.0 mm, 0.26–0.55 pix and 2.6–5.0 mm, respectively; Table 1);
3. The mean M3C2 uncertainty for the 2018–2025 comparison (1.43 mm), i.e., between models acquired with different cameras, falls within the range for comparisons between models acquired with the same camera (1.34–1.91 mm; Table 3).

These values are one to two orders of magnitude smaller than the detected changes, so a substantial influence of the camera change on the results is unlikely; nevertheless, residual systematic effects from the different sensor and lens cannot be fully excluded without a direct comparison of both set-ups.

6. Conclusions

This study compared three methods of evaluating the changes of a vertical ice wall in Dobšiná Ice Cave, applied to one series of seven SfM photogrammetric epochs (2018–2023 and 2025). The main conclusions are as follows:

1. All three methods independently confirmed a predominant retreat of the ice wall. By 2025, the mean retreat on the cross-sections reached 113 mm, the mean M3C2 distance reached −69.9 mm, and the vectorised glacial layers shifted by 72–214 mm. The only exception was a zone of local ice accumulation caused by water dripping from the cave ceiling, identified consistently by both the cross-sections and M3C2.
2. The methods agree in the order of magnitude of the change (units to low tens of millimetres per year). The differences between their values reflect different spatial sampling, not a discrepancy between the methods: the cross-sections and vectorisation capture local maxima at selected locations, whereas M3C2 averages the change over the entire wall.
3. Each method has a distinct role. M3C2 provides the most complete area-wide assessment, including measurement uncertainty and statistical significance, but depends most on the quality and density of the input point clouds. Cross-sections are the simplest tool for rapid inspection at predefined locations but miss changes outside the profiles. Vectorisation yields a stratigraphically interpretable record of individual layers but is labour-intensive and limited to the vectorised layers.

For long-term monitoring of vertical cave ice walls, M3C2 is best suited as the primary method, complemented by cross-sections for rapid inspection and vectorisation for layer-based interpretation. Together, they provide a more reliable basis for decisions on cave ice protection than any single method.

7. Future Research

Future research should focus on three directions. First, since the ice wall is not only retreating but also moving, as indicated by the displacement of the anchor monumented in the wall by 2–3 cm per year [12], the surface-normal change quantified by M3C2 combines ablation and ice flow. Tracking vectorised layers and image features in orthophotomosaics from successive epochs could provide displacement vectors and thus separate these two components. Second, the uncertainty of SfM-based change detection on cave ice should be quantified empirically. This can be achieved by repeating same-day image acquisitions, evaluating stable rock surfaces surrounding the wall, and, following the camera system change in 2025, directly comparing both setups within a single epoch. Reintroducing spring epochs would facilitate distinguishing winter accumulation from summer ablation, and linking the results to speleoclimatic records could help explain the observed interannual variability. Third, the labour-intensive manual vectorisation could be automated by edge detection or semantic segmentation of the layers in orthophotos. The approach could also be extended to other ice faces in Dobšiná Ice Cave and other ice caves, and applied backwards in time using historical photographs of the corridor.

Author Contributions: Conceptualisation, J.Š. and K.B.; methodology, K.P.; software, Ľ.K.; validation, K.P. and Ľ.K.; formal analysis, J.Š.; investigation, J.Š. and K.B.; resources, K.P.; data curation, Ľ.K.; writing—original draft preparation, J.Š.; writing—review and editing, J.Š. and K.B.; visualisation, J.Š. and K.B.; supervision, K.P. and Ľ.K.; project administration, K.P. and K.B.; funding acquisition, K.P. All authors have read and agreed to the published version of the manuscript.

Funding: This study is the result of the Grant Project of the Ministry of Education of the Slovak Republic KEGA No. 034TUKE-4/2026 and 018TUKE-4/2026 and VEGA No. 1/0231/26.

Data Availability Statement: Dataset available on request from the authors.

Acknowledgments: The authors thank the Slovak Caves Administration for permission to carry out measurements in Dobšiná Ice Cave and for providing the air temperature and humidity data from the Ruffínyi Corridor, and Ľubomír Očkaik, for his assistance during fieldwork. During the preparation of this manuscript, the authors used Claude (Anthropic; Claude Opus 5.5) for the purposes of language editing, formatting of references and editing of figure labels. The authors have reviewed and edited the output and take full responsibility for the content of this publication.

Conflicts of Interest: The authors declare no conflicts of interest. The funders had no role in the design of the study; in the collection, analyses, or interpretation of data; in the writing of the manuscript; or in the decision to publish the results.

Abbreviations

The following abbreviations are used in this manuscript:

M3C2	Multiscale Model-to-Model Cloud Comparison
SfM	Structure-from-Motion
DSLR	Digital Single-Lens Reflex
GNSS	Global Navigation Satellite System
SKPOS	Slovak real-time positioning service
S-JTSK	Datum of Uniform Trigonometric Cadastral Network
Bpv	Baltic Vertical Datum—After Adjustment
GPR	Ground-penetrating radar

References

1. Luetscher, M.; Jeannin, P.-Y. A process-based classification of alpine ice caves. *Theor. Appl. Karstol.* **2004**, *17*, 5–10.
2. Luetscher, M.; Jeannin, P.-Y.; Haeberli, W. Ice caves as an indicator of winter climate evolution: A case study from the Jura Mountains. *Holocene* **2005**, *15*, 982–993. [CrossRef]
3. Bădăluţă, C.-A.; Perşoiu, A.; Ionita, M.; Piotrowska, N. Stable isotopes in cave ice suggest summer temperatures in east-central Europe are linked to Atlantic Multidecadal Oscillation variability. *Clim. Past* **2020**, *16*, 2445–2458. [CrossRef]
4. Obleitner, F.; Trüssel, M.; Spötl, C. Climate warming detected in caves of the European Alps. *Sci. Rep.* **2024**, *14*, 27435. [CrossRef] [PubMed]
5. Securo, A.; Forte, E.; Martinucci, D.; Pillon, S.; Colucci, R.R. Long-term mass-balance monitoring and evolution of ice in caves through structure from motion–multi-view stereo and ground-penetrating radar techniques. *Prog. Phys. Geogr. Earth Environ.* **2022**, *46*, 422–440. [CrossRef]
6. Gómez-Lende, M.; Berenguer, F.; Serrano, E. Morphology, ice types and thermal regime in a high mountain ice cave. First studies applying terrestrial laser scanner in the Peña Castil ice cave (Picos de Europa, Northern Spain). *Geogr. Fis. Din. Quat.* **2014**, *37*, 141–150. [CrossRef]
7. Perşoiu, A.; Pazdur, A. Ice genesis and its long-term mass balance and dynamics in Scărişoara Ice Cave, Romania. *Cryosphere* **2011**, *5*, 45–53. [CrossRef]
8. Šupinský, J.; Kaňuk, J.; Hochmuth, Z.; Gallay, M. Detecting dynamics of cave floor ice with selective cloud-to-cloud approach. *Cryosphere* **2019**, *13*, 2835–2851. [CrossRef]
9. Veda na dosah. Pred 150 Rokmi Začal Výskum Dobšinskej ľadovej Jaskyne. (In Slovak) Available online: https://vedana-dosah.cvtisr.sk/priroda/zem/pred-150-rokmi-zacal-vyskum-dobsinskej-ladovej-jaskyne/ (accessed on 22 September 2026).
10. Gradziński, M.; Hercman, H.; Pereswiet-Soltan, A.; Zelinka, J.; Jelonek, M. Radiocarbon dating of fossil bats from Dobšina Ice Cave (Slovakia) and potential palaeoclimatic implications. *Ann. Soc. Geol. Pol.* **2016**, *86*, 341–350. [CrossRef]
11. Jelonek, M.; Pawlak, J.; Pereswiet-Soltan, A.; Zelinka, J.; Gradziński, M. Growth rate of cave ice based on ^{14}C dating of fossil bats as a palaeoenvironmental proxy for the last 1300 years in the Western Carpathians. *Holocene* **2025**, *35*, 1002–1014. [CrossRef]
12. Pukanská, K.; Bartoš, K.; Gašinec, J.; Pašteka, R.; Zahorec, P.; Papčo, J.; Bella, P.; Andrássy, E.; Dušeková, L.; Bobíková, D.; et al. Methodological approaches to survey complex ice cave environments—The case of Dobšiná (Slovakia). *Front. Environ. Sci.* **2024**, *12*, 1484169. [CrossRef]
13. Zelinka, J. Speleoklimatický a glaciologický výskum a monitoring od roku 1990. *Aragonit* **2009**, *14*, 104–109. (In Slovak) Available online: https://www.ssj.sk/sk/user_files/Aragonit14_2_komplet.pdf (accessed on 30 September 2026).
14. Pukanská, K.; Bartoš, K.; Bella, P.; Gašinec, J.; Blistan, P.; Kovanič, Ľ. Surveying and High-Resolution Topography of the Ochtiná Aragonite Cave Based on TLS and Digital Photogrammetry. *Appl. Sci.* **2020**, *10*, 4633. [CrossRef]
15. Bartoš, K.; Pukanská, K.; Kseňak, Ľ.; Gašinec, J.; Bella, P. Cross-Polarized SfM Photogrammetry for the Spatial Reconstruction of Challenging Surfaces, the Case Study of Dobšiná Ice Cave (Slovakia). *Remote Sens.* **2023**, *15*, 4481. [CrossRef]
16. Lague, D.; Brodu, N.; Leroux, J. Accurate 3D comparison of complex topography with terrestrial laser scanner: Application to the Rangitikei canyon (N-Z). *ISPRS J. Photogramm. Remote Sens.* **2013**, *82*, 10–26. [CrossRef]
17. Kern, Z. Dating cave ice deposits. In *Ice Caves*; Perşoiu, A., Lauritzen, S.-E., Eds.; Elsevier: Amsterdam, The Netherlands, 2018; pp. 109–122. [CrossRef]
18. Dušeková, L.; Herich, P.; Pukanská, K.; Bartoš, K.; Kseňak, Ľ.; Šveda, J.; Fehér, J. Comparison of Non-Contact Measurement Technologies Applied on the Underground Glacier—The Choice for Long-Term Monitoring of Ice Changes in Dobšiná Ice Cave. *Remote Sens.* **2024**, *16*, 3870. [CrossRef]
19. Blatnik, M.; Obu, J.; Košutnik, J.; Gabrovšek, F. Use of Terrestrial LiDAR Scanner for Monitoring of Ice Thickness in Ice Caves; Examples from Slovenia. In *EuroKarst 2022, Málaga*; Advances in Karst Science; Springer: Cham, Switzerland, 2023; pp. 185–192. [CrossRef]
20. Williams, J.G.; Anders, K.; Winiwarter, L.; Zahs, V.; Höfle, B. Multi-directional change detection between point clouds. *ISPRS J. Photogramm. Remote Sens.* **2021**, *172*, 95–113. [CrossRef]
21. Holmlund, P.; Onac, B.P.; Hansson, M.; Holmgren, K.; Mörth, M.; Nyman, M.; Perşoiu, A. Assessing the palaeoclimate potential of cave glaciers: The example of the Scărişoara Ice Cave (Romania). *Geogr. Ann. Ser. A Phys. Geogr.* **2005**, *87*, 193–201. [CrossRef]
22. Pfeiffer, J.; Rutzinger, M.; Spötl, C. Terrestrial laser scanning for 3D mapping of an alpine ice cave. *Photogramm. Rec.* **2023**, *38*, 6–21. [CrossRef] [PubMed]
23. Brun, F.; Buri, P.; Miles, E.S.; Wagnon, P.; Steiner, J.; Berthier, E.; Ragettli, S.; Kraaijenbrink, P.; Immerzeel, W.W.; Pellicciotti, F. Quantifying volume loss from ice cliffs on debris-covered glaciers using high-resolution terrestrial and aerial photogrammetry. *J. Glaciol.* **2016**, *62*, 684–695. [CrossRef]
24. Bella, P.; Tulis, J.; Zelinka, J.; Papáč, V.; Višňovská, Z.; Haviarová, D. Dobšiná Ice Cave (Slovakia, Central Europe) and its unique underground glacier originated in the mid-mountain position of the moderate climate zone. *Aragonit* **2020**, *25*, 4–16.

25. Slovakia Travel. Dobšinská ľadová Jaskyňa. Available online: https://slovakia.travel/dobsinska-ladova-jaskyna (accessed on 12 August 2022).
26. Gašinec, J.; Gašincová, S.; Gergeľová, M. Tvorba priestorového modelu Dobšinskej ľadovej jaskyne a jeho pripojenie na JTSK03. *Geod. Kartogr. Obz.* **2012**, *58*, 211–223. (In Slovak)
27. Seznam.cz. Mapy.com. Available online: https://mapy.com/en/letecka?x=20.3067898&y=48.8713051&z=16&m3d=1&height=2474&yaw=124&pitch=-46 (accessed on 27 September 2026).
28. Caroig. Slovakia—Outline Map [Vector Map]; Wikimedia Commons, 2007; CC BY-SA 3.0. Available online: https://commons.wikimedia.org/wiki/File:Slovakia_-_outline_map.svg (accessed on 30 September 2026).
29. Droppa, A. Dobšinská ľadová jaskyňa. *Geogr. Čas.* **1957**, *9*, 99–118. (In Slovak)
30. Správa Slovenských Jaskýň. Dobšinská ľadová Jaskyňa. Available online: https://www.ssj.sk/sk/jaskyna/6-dobsinska-ladova-jaskyna (accessed on 28 September 2026). (In Slovak)
31. May, B.; Spötl, C.; Wagenbach, D.; Dublyansky, Y.; Liebl, J. First investigations of an ice core from Eisriesenwelt cave (Austria). *Cryosphere* **2011**, *5*, 81–93. [CrossRef]
32. Perşoiu, A.; Onac, B.P.; Perşoiu, I. The interplay between air temperature and ice mass balance changes in Scărişoara Ice Cave, Romania. *Acta Carsol.* **2011**, *40*, 445–456. [CrossRef]
33. Westoby, M.J.; Brasington, J.; Glasser, N.F.; Hambrey, M.J.; Reynolds, J.M. 'Structure-from-Motion' photogrammetry: A low-cost, effective tool for geoscience applications. *Geomorphology* **2012**, *179*, 300–314. [CrossRef]
34. Remondino, F.; Spera, M.G.; Nocerino, E.; Menna, F.; Nex, F. State of the art in high density image matching. *Photogramm. Rec.* **2014**, *29*, 144–166. [CrossRef]
35. CloudCompare, Version 2.14.beta [GPL Software]. 2026. Available online: https://www.cloudcompare.org/ (accessed on 30 June 2026).
36. Hochmuth, Z.; Šupinský, J.; Stankovič, J.; Halama, J.; Kaňuk, J. Dynamics of temperature changes in the Silická Ľadnica Cave (Slovak karst) and its influence on the ice accumulations. *Aragonit* **2020**, *25*, 42–43. Available online: https://www.ssj.sk/user_files/Aragon_25_1_web1.pdf (accessed on 30 September 2026).
37. Šupinský, J.; Nováková, M.; Gallay, M.; Kaňuk, J. Microclimatic and ice accumulation change monitoring in Silická ľadnica cave. In Proceedings of the 10th International Workshop on Ice Caves (IWIC-X), Werfenweng, Austria, 12–18 May 2024; p. 39.

Disclaimer/Publisher's Note: The statements, opinions and data contained in all publications are solely those of the individual author(s) and contributor(s) and not of MDPI and/or the editor(s). MDPI and/or the editor(s) disclaim responsibility for any injury to people or property resulting from any ideas, methods, instructions or products referred to in the content.